

RESEARCH ARTICLE

Dietary limonene promotes gastrointestinal barrier function via upregulating tight/adherens junction proteins through cannabinoid receptor type-1 antagonistic mechanism and alters cellular metabolism in intestinal epithelial cells

K. J. Senthil Kumar^{1,2}  | M. Gokila Vani³  | Gyaltzen Dakpa^{4,5} | Sheng-Yang Wang^{3,4,6,7} 

¹Bachelor Program of Biotechnology, National Chung Hsing University, Taichung, Taiwan

²Center for General Education, National Chung Hsing University, Taichung, Taiwan

³Department of Forestry, National Chung Hsing University, Taichung, Taiwan

⁴Molecular and Biological Agricultural Sciences Program, Taiwan International Graduate Program, Academia Sinica, Taipei, Taiwan

⁵Graduate Institute of Biotechnology, National Chung Hsing University, Taichung, Taiwan

⁶Agricultural Biotechnology Research Center, Academia Sinica, Taipei, Taiwan

⁷Special Crop and Metabolome Discipline Cluster, Academy of Circle Economy, National Chung Hsing University, Taichung, Taiwan

Correspondence

Sheng-Yang Wang, Department of Forestry, National Chung Hsing

Abstract

Limonene, a dietary monocyclic monoterpene commonly found in citrus fruits and various aromatic plants, has garnered increasing interest as a gastrointestinal protectant. This study aimed to assess the effects of limonene on intestinal epithelial barrier function and investigate the involvement of cannabinoid receptor type-1 (CB1R) *in vitro*. Additionally, the study focused on examining the metabolomic changes induced by limonene in the intestinal epithelial cells (Caco-2). Initial analysis of transepithelial electrical resistance (TEER) revealed that both *L*-limonene and *D*-limonene, isomers of limonene, led to a dose- and time-dependent increase in TEER in normal cells and those inflamed by pro-inflammatory cytokines mixture (CytoMix). Furthermore, both types of limonene reduced CytoMix-induced paracellular permeability, as demonstrated by a decrease in Lucifer yellow flux. Moreover, *D*-limonene and *L*-limonene treatment increased the expression of tight junction molecules (TJs) such as occludin, claudin-1, and ZO-1, at both the transcriptional and translational levels. *D*-Limonene upregulates E-cadherin, a molecule involved in adherens junctions (AJs). Mechanistic investigations demonstrated that *D*-limonene and *L*-limonene treatment significantly inhibited CB1R at the protein, while the mRNA level remained unchanged. Notably, the inhibitory effect of *D*-limonene on CB1R was remarkably similar to that of pharmacological CB1R antagonists,

Abbreviations: ¹H-NMR, proton nuclear magnetic resonance; 2-AG, 2-arachidonoylglycerol; AJs, adhesion junction molecules; BMRB, the biological magnetic resonance data bank; CB1R, cannabinoid receptor 1; cDNA, complementary DNA; CytoMix, cytokines mixture; DMEM, Dulbecco's modified Eagle medium; ECL, enhanced chemiluminescence; ELISA, enzyme-linked immunosorbent assay; ERK1/2, the extracellular signal-regulated kinase 1/2; FBS, fetal bovine serum; FC, fold change; GAPDH, glyceraldehyde 3-phosphate dehydrogenase; HRP, horseradish peroxidase; IL-1 β , interleukin 1 β ; INF- γ , interferon- γ ; JAM-1,2, junction adhesion molecules-1, 2; LPS, lipopolysaccharide; LY, lucifer yellow; MPER, mammalian protein extraction reagent; mRNA, messenger RNA; MSEA, metabolite set enrichment analysis; MTT, (3-(4,5-dimethylthiazol-2-yl)-2,5-diphenyltetrazolium bromide); MVDA, multivariate data analysis; PLS-DA, partial least squares-discriminant analysis; PVDF, polyvinylidene fluoride or polyvinylidene difluoride; Q-PCR, quantitative polymerase chain reaction; Sc_siRNA, scrambled siRNA; SD, standard deviation; SDS-PAGE, sodium dodecyl-sulfate polyacrylamide gel electrophoresis; siCB1R, CB1R siRNA; TEER, trans-epithelial electrical resistance; TJs, tight junction molecules; TNF- α , tumor necrosis factor- α ; TSP, trimethylsilylpropanoic acid; VIP, variable importance of projection; ZO-1,2, and 3, Zonula occludens-1, 2, and 3.

University, Taichung 402, Taiwan.
Email: taiwanfir@dragon.nchu.edu.tw

Funding information

Theaceae Conservation Corporation,
Grant/Award Number: 109D593; National
Science and Technology Council,
Grant/Award Number: 109-2313-B-
005-043-MY3

such as rimonabant and ORG27569. D-limonene also alters Caco-2 cell metabolites. A substantial reduction in β -glucose and 2-succinamate was detected, suggesting limonene may impact intestinal epithelial cells' glucose uptake and glutamate metabolism. These findings suggest that D-limonene's CB1R antagonistic property could effectively aid in the recovery of intestinal barrier damage, marking it a promising gastrointestinal protectant.

KEYWORDS

adherence junction, CB1R, intestinal epithelial cells, limonene, metabolites, tight junction

1 | INTRODUCTION

Limonene, a prevalent monocyclic monoterpene abundantly found in nature, serves as a primary component in various essential oils derived from citrus fruits, coniferous trees, and broad-leaved plants.¹ It exists as a clear liquid with two optical isomers: D-limonene and L-limonene, or it can also be found as a racemic mixture. D-Limonene, occurs more commonly in nature, imparting the fragrance of citrus fruits, while L-limonene is less common and is found in the edible parts of such plants as caraway, dill, bergamot orange, citronella, and lemongrass.^{2,3} Limonene finds extensive use as a cost-effective fragrance in cosmetics and is present in various beauty products such as soaps, perfumes, shampoos, hair conditioners, shower gels, cleaning agents, and environmentally friendly pesticides.⁴ Extensive research has investigated the therapeutic properties of limonene, demonstrating its antioxidant, anti-inflammatory, anticancer, antiviral, antinociceptive, antidiabetic, gastroprotective, and anti-hyperalgesia effects.⁵ Following oral intake, limonene undergoes quick absorption in the gastrointestinal tract, distribution, and metabolism. It is considered safe for human consumption, exhibiting low toxicity and posing no mutagenic, carcinogenic, or nephrotoxic risks to humans.⁶

The gastrointestinal epithelium, also known as the intestinal barrier, serves as a selectively permeable structure that facilitates the passage of water, electrolytes, and essential dietary nutrients, while effectively preventing the diffusion of pathogens, toxins, and allergens from the intestinal lumen into the bloodstream.⁷ A defect in the integrity of the intestinal barrier integrity is associated with various pathological conditions, including metabolic disorders, obesity, inflammatory bowel disease, and irritable bowel syndrome.⁸ The defense of the intestine is influenced by interactions among several barrier components, including the mucosal membrane, mucosal immune system, adhesion molecules, adherens junctions (AJs), tight junctions (TJs), and desmosomes. Among

these components, the AJs and TJs play a critical role as the major determinants of the intestinal physical barrier and its integrity. AJs consists catenins (α -catenin, catenin 1 β , δ -catenin, and γ -catenin) and cadherins (E-cadherin and N-cadherin), which regulate the mechanical linkage of adjacent cells. On the other hand, TJs comprise occludin and claudins 1–12, and junctional adhesion molecules (JAM-1 and JAM-2), forming an apical junctional complex that seals the intercellular space and modulates selective paracellular permeability. The intracellular domains of AJs, TJs, and JAMs interact with cytoplasmic scaffold proteins, such as zonula occludin (ZO-1, ZO-2, and ZO-3), which anchor the transmembrane proteins to the prejunctional actomyosin ring. The interplay between TJ proteins and the actin cytoskeleton is of utmost importance in maintaining the integrity and functionality of TJs, including their permeability characteristics.

Cannabinoid receptors (CBRs) are G-protein coupled receptors belonging to the rhodopsin-like subfamily that mediate the biological effects of phyto-cannabinoids, endocannabinoids, and synthetic cannabinoids. These CBRs are highly expressed in nearly all mammalian tissues. Several studies have demonstrated up-regulation of CBRs in different inflammatory conditions. Notably, elevated CB1R expression was observed in mice with croton oil-induced inflammation of the small intestine,⁹ while CB2R overexpression was found in colonic tissues in inflammatory bowel disease patients.¹⁰ Studies have demonstrated the advantageous effects of cannabinoids in managing various gastrointestinal disorders through the regulation of CBRs. A recent study has shown that cannabidiol treatment inhibits *Clostridium difficile* toxin A-induced apoptosis and improves intestinal barrier integrity in Caco-2 cells, involving the CB1R.¹¹ Confluent Caco-2 cells, exhibiting morphological and biological traits resembling small intestinal enterocytes, such as brush-border microvilli, TJs, and dome formation. Due to these features, serve as an appealing model for investigating intestinal permeability.¹² In our recent study, we demonstrated that pre-treatment of limonene provides

protection to skin keratinocytes against photodamage and photoaging induced by ultraviolet radiation. Although the effect did not reach statistical significance. The protective mechanism was linked to an improvement in barrier function by increasing the expression of TJ proteins, including occludin and ZO-1.¹³ Additionally, another study reported that essential oils derived from lemon and limonene exhibit protective effects in mice against *Escherichia coli*-induced intestinal injury and inflammation,¹⁴ though the precise underlying mechanisms remain unclear. Thus, the objective of the current study was to explore the impact of limonene on barrier function in intestinal epithelial cells and elucidate the underlying molecular mechanisms.

Several experimental studies can shed light on cellular metabolic changes through the incorporation of various metabolomic methodologies, molecular-level investigations, and integrative analyses of “omic” data, encompassing proteomics and genomics-scale studies.¹⁵ A comprehensive investigation into cellular metabolism can yield valuable insights into biological systems. The significance of cell metabolomics has increasingly been recognized in elucidating cellular metabolite profiles and characterizing disrupted metabolic pathways. These metabolites typically represent the final downstream products of gene transcription, implying that any alterations to them are likely to be amplified.¹⁶ In the meantime, identifying of metabolic correction could serve as a potential indicator of enzymatic activities, thereby providing insights into the pharmacological activities and mechanism of small molecules.¹⁷ Consequently, the objective of this study was also to examine the changes in cellular metabolism induced by D-limonene on intestinal epithelial cells in an in vitro setting.

2 | EXPERIMENTAL PROCEDURES

2.1 | Chemical and reagents

The Dulbecco's modified Eagle medium/F-12 nutrient mixture (DMEM/F12), fetal bovine serum (FBS), penicillin, and streptomycin were acquired from Life Technologies, Grand Island, NY. The 3-(4,5-dimethyl-thiazol-2-yl)-2,5-diphenyl tetrazolium bromide (MTT), 2-arachidonoylglycerol (2-AG), and methanol-d₄ (>99.8 atom% D) containing trimethylsilyl propionic acid sodium salt (TSP) were obtained from Sigma-Aldrich in St. Louis, MO. Rimonabant (Rim) and ORG-27569 (ORG) were obtained from Selleckchem (Houston, TX). Antibody against occludin (65 kDa, #91131), claudin (20 kDa, #4933), ZO-1 (220 kDa, #13663), E-cadherin (135 kDa, #3195), vimentin (57 kDa, #5741), CB1R (60 kDa,

#93815), and HRP-linked anti-rabbit IgG (#7074) and anti-mouse IgG (#7076) anti-bodies were purchased from Cell Signaling Technology (Danvers, MA). β -actin (43 kDa, sc-47778) and GAPDH (36 kDa, sc-47724) were purchased from Santa-Cruz Biotechnology, Dallas, TX. Analytical grade methanol (MeOH) for liquid chromatography was purchased Merck (Darmstadt, Germany), respectively.

2.2 | Cell culture

Caco-2 cells were obtained from the American Type Culture Collection (Rockville, MD). Cells were cultured in DMEM/F12 medium supplemented with 10% FBS, 2 mM L-glutamine, 100 IU/mL penicillin, and streptomycin and incubated in a humidified atmosphere containing 5% CO₂ at 37°C.

2.3 | Cell viability assay

Cell viability was evaluated using the MTT colorimetric assay. In summary, Caco-2 cells were cultured in a 24-well plate at a density of 5×10^4 cells/well. After 48 h of incubation, the cells were incubated with different concentrations (25, 50, 100, 150, and 200 μ M) of D-/L-limonene for an additional 48 h. Control cells were incubated with 0.1% DMSO/F-12 for 48 h. After removing the cell culture supernatant, 1 mg/mL of MTT in 0.4 mL fresh culture medium was introduced. The resulting MTT formazan crystals were dissolved in 0.4 mL of DMSO. Subsequently, the samples were measured at 570 nm (A_{570}) with the help of an ELISA microplate reader (Bio-Tek Instruments, Winooski, VT). To determine the percentage of cell viability, the following formula was used: (A_{570} of treated cells/ A_{570} of untreated cells) \times 100.

2.4 | Trans-epithelial electrical resistance and Lucifer yellow flux assays

To evaluate the integrity of the monolayer, the trans-epithelial electrical resistance (TEER) was measured using an Evometer (Evom, World Precision Instruments; Hertfordshire, UK) equipped with “chopstick” electrodes. Caco-2 cells (5×10^4 cells/well) were placed onto permeable polyester membrane filter supports (24-well Millicell hanging cell culture insert with a pore size of 8.0 μ m) and cultured for 18–20 days prior to experimentation, with the culture medium refreshed every other day. For the subsequent experiments, a fully formed monolayer of cells with an epithelial resistance above 1000 Ω -cm² was utilized. With the exception of the control group, cells in

all other groups were pre-treated with varying concentrations of D-/L-limonene, or Rim or ORG, either alone or in combination with CytoMix (a cocktail of pro-inflammatory mediators consisting 50 ng/mL TNF- α , 25 ng/mL IL-1 β , 50 ng/mL IFN γ were applied to the basolateral compartment and 1 μ g/mL lipopolysaccharide (LPS) and 2-AG were applied to both the apical and basolateral compartments for 48 h). In this incubation period, epithelial resistance was measured at various time points (6, 12, 24, and 48 h). A cell-free insert was utilized as a reference, and its average resistance was subtracted from all the samples. Each well was measured three times, and the resulting average resistance value was calculated. All experiments were conducted 18–20 days post-seeding. Cultures within passages 35 to 60 were employed, and the culture medium was renewed every 3 days. To determine paracellular permeability, 100 μ M Lucifer yellow (LY; ThermoFisher Scientific Inc., Waltham, MA) were added onto the apical wells at 48 h post-administration and the fluxes into the basal wells were assessed for 3 h. LY concentration in the basal wells were determined by measuring fluorescent intensity with a spectrophotometer (Hidex Oy, Turku, Finland). The excitation and emission wavelengths were 430 and 540 nm, respectively.

2.5 | Preparation of whole cells and detergent-insoluble protein fractions

The whole cell lysate was prepared using mammalian protein extraction reagent (MPER) from Pierce Biotechnology, Rockford, IL. Detergent-insoluble fraction was obtained by utilizing cytoplasmic, nuclear, and pellet protein extraction reagents (Pierce Biotechnology). Briefly, Caco-2 cell monolayers treated with limonene, Rim, ORG, or 2-AG in the presence or absence of CytoMix were washed with ice-cold PBS and incubated for 5 min at 4°C with 200 mL of MPER buffer containing protease and phosphatase inhibitors. Cell lysates were centrifuged at 16,000g for 10 min at 4°C to sediment the high-density actin-rich fraction, which is whole cell extract. Next, the sedimented pellet was resuspended in 100 μ L of pellet protein extraction buffer containing protease and phosphatase inhibitors. The supernatant obtained from this step represented the detergent-insoluble fraction. Protein concentrations were determined using the Bio-Rad protein assay reagent (Bio-Rad Laboratories, Hercules, CA).

2.6 | Immunoblotting

Equal amounts of protein samples (60–100 μ g) were electrophoresed using 8–12% SDS-PAGE, and the separated

proteins were then transferred onto a polyvinylidene fluoride (PVDF) membrane overnight. After the transfer, the protein membranes were blocked with 5% non-fat skim milk for 30 min. Next, the membranes were incubated with specific primary antibodies, including occludin, claudin, ZO-1, E-cadherin, vimentin, CB1R, β -actin, and GAPDH for overnight, followed by HRP-conjugated anti-rabbit or anti-mouse secondary antibodies for 2 h. The immunoblots were developed using enhanced chemiluminescence (ECL) reagents from Advansta Inc (San Jose, CA). The images were captured using the ChemiDoc XRS⁺ docking system, and the protein bands were quantified using Imagelab software from Bio-Rad Laboratories, Hercules, CA.

2.7 | RNA extraction and q-PCR analyses

Total RNA was isolated from cultured Caco-2 cells using a total RNA purification kit from GeneMark, New Taipei City, Taiwan. The concentration of total RNA was determined using a NanoVue Plus spectrophotometer (GE Health Care Life Sciences, Chicago, IL). Real-time PCR was conducted using a real-time PCR detection system and software (Applied Biosystems, Foster City, CA). First-strand cDNA was synthesized using the SuperScript IV reverse transcriptase kit from Invitrogen. To quantify mRNA expression of the genes of interest, qPCR reactions were performed with an equal volume of cDNA, forward and reverse primers (10 μ M), and power SYBR Green Master Mix from Applied Biosystems. GAPDH was used for mRNA level normalization. The primer sequences for qPCR were designed by TRiBiotech in Hsinchu, Taiwan, and are summarized in Table S1.

2.8 | CB1R knockdown via siRNA

siRNA transfection utilized Lipofectamine RNAiMax (Invitrogen) in accordance with the manufacturer's guidelines. Caco-2 cells were cultivated in DMEM/F-12 medium supplemented with 10% FBS, seeded in 6-well plates, and allowed to incubate for to reach a monolayer with over 90% confluence at the time of transfection. Following this, the culture medium was substituted with 500 μ L of Opti-MEM (Invitrogen), and cells underwent transfection using the RNAiMAX transfection reagent. For each transfection, 5 μ L of RNAiMAX was blended with 250 μ L of Opti-MEM and incubated for 5 mi at room temperature. Simultaneously, scrambled siRNA or siCB1R (100 pM, resulting in a final concentration of 100 nM in 1 mL Opti-MEM) was combined with 250 μ L of Opti-MEM. The siRNA solution was then introduced

to the diluted RNAiMAX reagent. The resulting siRNA/RNAiMAX mixture (500 μ L) was incubated for an additional 25 min at room temperature to facilitate complex formation. Subsequently, the solution was added to the cells in the 6-well plates, resulting in a final transfection volume of 1 mL. After a 6 h incubation, the transfection medium was replaced with 2 mL of standard growth medium, and the cells were cultured at 37°C. Following a 24 h transfection, the cells were treated with D-limonene (100 μ M) and induced by CytoMix for 24 h. Subsequent to this treatment, RNA extraction and Q-PCR analysis were performed.

2.9 | Preparation of cellular metabolites

Following the treatment, the culture media was removed, and the cells were washed three times with PBS. Then, 2 mL of trypsin was used to harvest the cells, which were subsequently suspended in 2 mL of fresh PBS. The cell suspension was transferred to a 2 mL centrifuge tube and centrifuged for 5 min at 500g at 4°C. After aspirating the supernatant, the resulting cell pellet was stored at -80°C until the extraction process began. To extract cellular metabolites, the pellet cells were sonicated on ice for 10 s at 60% intensity using the Ultrasonic Processor/UP-800 (Chrome tech in Apple Valley, CA). For this extraction, cold 90% methanol was employed, following a previously described method by Ref. [18], with some modifications, as no standardized protocol is available for metabolite extraction from the cells similar to protein or RNA extraction. Specifically, 800 μ L of the extraction solvent (90% methanol) was added to the tube containing the cell pellet. The tube was then vortexed on ice for 10 min and centrifuged at 10,000g for 15 min at 4°C. The resulting supernatant was transferred to fresh tubes and stored at -80°C for further evaluation or the continuation of drying samples for subsequent assessments. The supernatant was later moved to new tubes and dried using a vacuum drier. Once the samples were dried, they were normalized for metabolic study. Additionally, the obtained cell pellets were kept at -80°C for further experiments. Throughout all the cell handling procedures, the work was performed on ice unless specified otherwise. A detailed protocol can be found in Figure S1.

2.10 | Cell normalization and sample preparation for $^1\text{H-NMR}$ analysis

Cell-based metabolomics requires the analysis of cell metabolomes from different groups. To ensure accurate

comparisons, the sample amount must be normalized before conducting NMR. This study aimed to perform comparative measurements of metabolite levels in distinct cell groups. To achieve this, an identical number of cells (5×10^5 cells/mL) was seeded in each 10 cm culture dish, ensuring equal amounts for harvesting and initial substance extraction from each well.¹⁹ Three independent experiments were conducted. After drying the samples, the cell extract was resuspended in 600 μ L of the methanol- d_4 solution containing the TSP (0.1% w/v). Subsequently, all samples were vortexed and transferred into 5 mm NMR tubes.

The $^1\text{H-NMR}$ analysis was carried out on a Bruker Advance III-400 NMR spectrometer from Bruker Corp in Billerica, MA. The temperature was set and maintained at 25°C. During the initial NMR data acquisition, gradient shimming was performed using methanol- d_4 as an internal lock. The chemical shifts were referenced to the internal standard TSP, which was set as zero chemical shifts. Each sample underwent 1000 transient scans (Figures S2 and S3). The spectra were subsequently baseline-corrected, phase-corrected, and subjected to a line broadening factor of 1.0 Hz using TopSpin software (Bruker, Massachusetts). The binned integrals of the $^1\text{H-NMR}$ data were exported to an Excel sheet for multivariate data analysis (MVDA). The intensity or integral of each spectrum was determined based on TSP as a reference value of 1. Overall, the spectra from the control and D-limonene groups appeared to be similar.

2.11 | Multivariate data analysis and metabolite characterization

The spectra were baseline-corrected, phase-corrected, and subjected to a line broadening factor of 1.0 Hz using TopSpin software (Bruker Corp). All spectra were binned and exported into a Window's Excel sheet for MVDA based on the binned integrals of the $^1\text{H-NMR}$ data. The intensity or integral of the spectrum was determined by TopSpin using TSP as the reference with an intensity value of 1. Further analysis was conducted using MetaboAnalyst 5.0, a web-based metabolomics analysis software with integrated R scripts (<https://www.metaboanalyst.ca>). Missing values were estimated using k-nearest neighbors, and metabolites with missing values in 50% or more samples were excluded. The data were then normalized by the sum of the total intensity and auto-log transformed for data normalization. In the subsequent two-sample *t*-test for each group, metabolites with a concentration change greater than 2-fold and a false discovery rate-adjusted *p*-value <0.05 were

considered significantly altered. For hierarchical clustering analysis, the distance measure used was Euclidean, and the clustering algorithm employed was ward. The groups were effectively separated using partial least squares discriminant analysis (PLS-DA) machine learning analysis. Metabolite set enrichment analysis (MSEA) and metabolic pathway analysis (MetPA) 5.0 were integrated for the analysis of over-represented metabolic pathways associated with the disease. To identify the metabolites, chemical shifts from online databases such as the human metabolome database (<https://hmdb.ca>) and Biological Magnetic Resonance Data Bank (BMRB) (<https://bmrbl.io>) were used, along with comparisons with previous literature and detailed metabolite references were presented in Table S2.

2.12 | Statistical analysis

The data is presented as the mean \pm standard deviation (SD). All statistical analyses were carried out using GraphPad Prism version 6.0 for Windows, a statistical software by GraphPad Software, La Jolla, CA. The analysis involved performing one-way ANOVA, followed by Dunnett's test for multiple comparisons. p values of $<0.01^{\Delta}$ was considered statistically significant for the CytoMix/2-AG treatment versus the control group. p values of $<0.05^*$, 0.01^{**} , and 0.001^{***} were considered statistically significant for the CytoMix/2-AG/control treatment versus D/L-limonene, rimonabant, or ORG-27569 treatment groups.

3 | RESULTS

3.1 | Assessment of limonene's cytotoxicity on Caco-2 cells

Before investigation the protective efficacy of limonene on the intestinal barrier function in Caco-2 cells, we evaluated potential cytotoxic effect of D-limonene and L-limonene. Caco-2 cells were exposed to various concentrations of D-/L-limonene (25, 50, 100, 150, and 200 μM) for 48 h, and the cell viability was measured using the MTT colorimetric assay. The results indicated that both D-limonene (Figure 1A) and L-limonene (Figure 1B) did not cause cytotoxicity up to a concentration of 100 μM for 48 h period. However, significant cytotoxicity was observed at concentration above 100 μM . Based on these findings, subsequent experiments conducted using non-cytotoxic concentrations of limonene specifically below 100 μM .

3.2 | Effect of limonene on healthy intestinal epithelial monolayers

In this study, we investigated the impact of D-limonene and L-limonene on an intact and non-stressed monolayer of Caco-2 cells. The changes in the TEER after incubation the cells with the test samples served as an indicator of potential effects. As a control group, cell monolayers incubated with 1% DMSO was used. TEER measurement were taken immediately after the incubation of the test samples and at regular intervals of 6 h (6, 12, and 24 h) until 24 h. Figure 1C, illustrates that treatment with D-limonene led to a significant increase in TEER in the of Caco-2 cell monolayer. TEER values started to gradually increase after 6 h and, at the end of treatment at 24 h, were significantly as well as dose-dependently by D-limonene. Notably, the TEER in monolayers incubated with 100 μM D-limonene increased to 111% of the initial value at 12 h, and further reached 154% at 24 h. Interestingly, the TEER value in monolayers treated with 25 μM D-limonene was higher than that of 50 μM D-limonene. Throughout the incubation period, the TEER in control cells exhibited ranged between 106% and 111%. Similarly, treatment with L-limonene also resulted in a significant increase in TEER in the Caco-2 cell monolayer. After 6 h of treatment, the TEER in all the L-limonene treatment groups began to rise. At 24 h, the TEER in cells treated with 50 μM L-limonene treatment increased to 121%, while 25 μM and 100 μM L-limonene increased to 107% and 117%, respectively. The TEER in control cells remained between 101% and 103% throughout the incubation period (Figure 1D). Additionally, the cell monolayers treated with 100 μM quercetin exhibited a gradual increase in TEER and peaked at 24 h (163.8%). Interestingly, treatment with 100 μM D-limonene led to a competitive increase in TEER (156.1%), while 100 μM L-limonene showed a moderately increased (120.8%) (Figure 1E). Overall, these findings suggest that, compared with L-limonene, D-limonene has a greater ability to enhance TJ integrity in intestinal epithelial cells.

3.3 | Effect of limonene on inflamed intestinal epithelial cell function

Subsequently, we aim to investigate the potential D-limonene and L-limonene in promoting the healing and recovery of inflamed epithelial cell monolayers. To induce stress or damage to the otherwise healthy monolayers, we exposed cells to a pro-inflammatory cytokine mixture (CytoMix) and measured the damage using

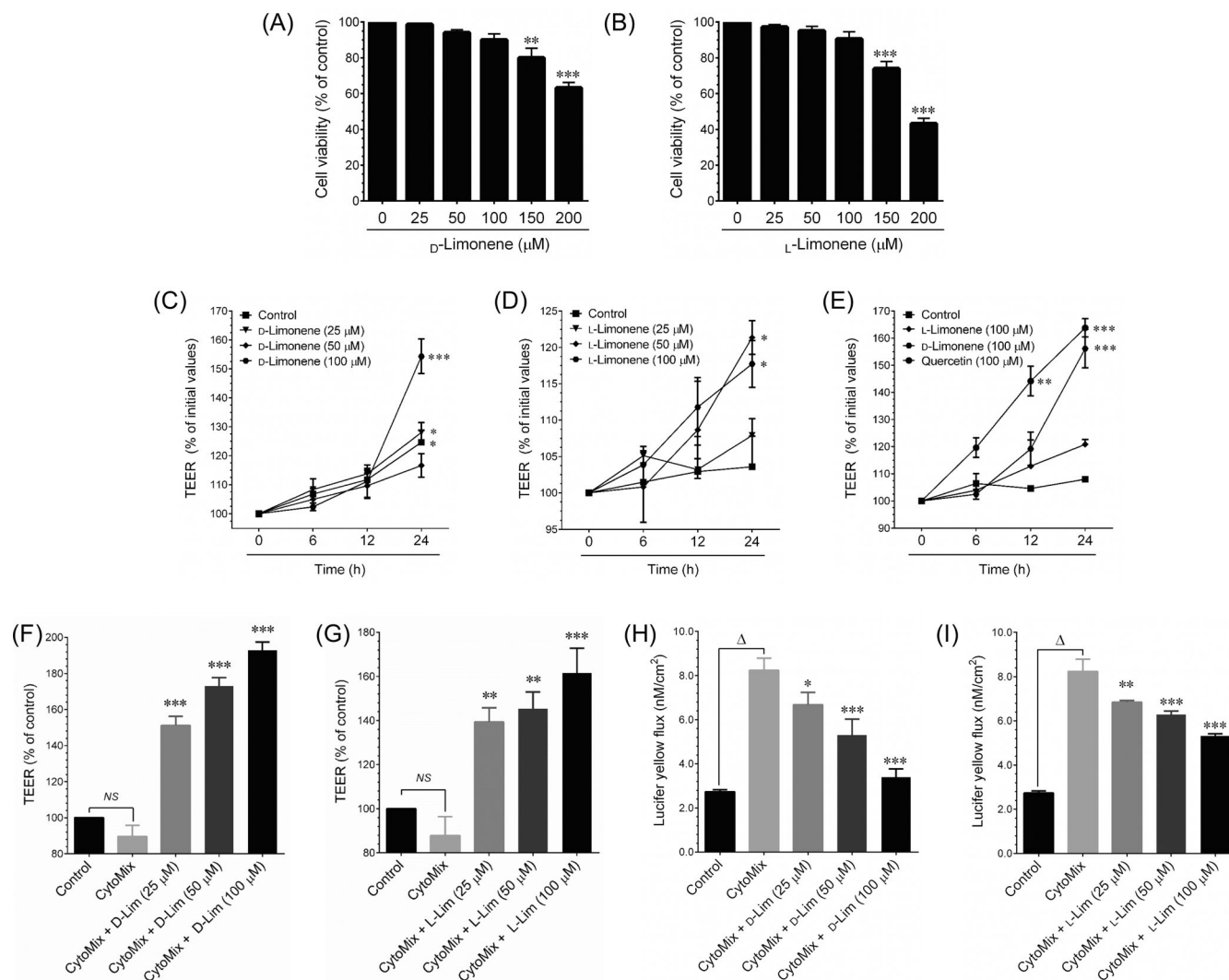


FIGURE 1 Cytotoxicity, TEER, and LY flux in Caco-2 cells incubated with D/L-limonene. Caco-2 cells were incubated with increasing doses of (A, B) D-limonene and (B) L-limonene for 48 h. Cell viability was assessed using the MTT assay, and the results were compared to the control group treated with 0.01% DMSO. The data presented are the mean ± SD of three independent experiments. Statistical significance was denoted as ***p* < 0.01 and ****p* < 0.001 when comparing the D/L-limonene treatment groups to the control group. (C-E) Caco-2 cell monolayers were incubated with increasing doses of D/L-limonene or quercetin. TEER was measured before and at 6, 12, and 24 h after the administration of D/L-limonene or quercetin. (F, G) The caco-2 cell monolayer barrier was disturbed by incubation with CytoMix and then treated with various doses of D/L-limonene for 24 h. TEER was measured at 24 h after the administration of CytoMix in the presence or absence of D/L-limonene. (H, I) Caco-2 cell monolayers were incubated with increasing doses of D/L-limonene for 3 h. LY flux fluorescent intensity was measured spectrophotometrically. ^Δ*p* < 0.001 compared to control versus CytoMix and **p* < 0.05, ***p* < 0.01, ****p* < 0.001 compared with CytoMix alone treatment group versus CytoMix + sample treatment groups.

TEER. Afterward, the cells were treated with varying doses of D-limonene and L-limonene, and the TEER values were recorded at 24 h after sample treatment. The untreated monolayers maintained their TEER level from 0 to 24 h, while the cells incubated with CytoMix significantly reduced in TEER of Caco-2 cells, ranging from to 36.2% to 38.6% after 24 h. Additionally, the cell monolayers damaged with CytoMix did not recover even when the medium was replaced a fresh one without CytoMix,

as evidenced by the unaltered TEER values. This strongly suggests that spontaneous recovery of the monolayer did not occur. Interestingly, co-treatment with either D-limonene or L-limonene led to a significant and dose-dependently increase in TEER values after 24 h of incubation. This effect was sustained for at least 12 h post-incubation. Specifically, treatment with D-limonene effectively restored the CytoMix-induced damage to the cell monolayers, as evidenced by the increase in TEER from

37.8% to 69.2%, 91.9%, and 114.9% with 25, 50, and 100 μM of D-limonene, respectively (Figure 1F). Similarly, treatment with L-limonene significantly increased TEER from 36.2% to 71.1%, 92.9%, and 129.5% by 25, 50, and 100 μM of L-limonene, respectively (Figure 1G).

3.4 | Effect of limonene on paracellular permeability of epithelial cell monolayers

In order to precisely determine and quantify changes in paracellular permeability, we employed the diffusion of LY as a widely accepted indicator. We measured LY flux to evaluate the protective effect of limonene on the integrity of Caco-2 cell monolayer. As indicated the TEER values, Caco-2 cell monolayers exposed to CytoMix showed a significantly increased LY diffusion and flux. The LY diffusion and flux increased from 2.73 nM/cm^2 in the control group to 8.23 nM/cm^2 after CytoMix treatment, indicating severe barrier damage caused by the CytoMix treatment. However, treatment with D-limonene significantly and dose-dependently reduced CytoMix-induced LY flux to 6.67 nM/cm^2 , 5.30 nM/cm^2 , and 3.39 nM/cm^2 at concentrations of 25, 50, and 100 μM , respectively (Figure 1H). A similar trend was observed in L-limonene-treated cells. Treatment with 25, 50, and 100 μM L-limonene significantly and dose-dependently restored LY flux to 6.84, 6.29, and 5.31 nM/cm^2 , respectively (Figure 1I). These data suggest that, compared with L-limonene, D-limonene has the potential to better ameliorates the disruption of the epithelial barrier function and caused by inflammatory cytokine insult in intestinal epithelial cells.

3.5 | Effect of limonene on TJ proteins in intestinal epithelial cells

To further investigate the changes in paracellular permeability on epithelial cell monolayers following CytoMix and limonene treatments, and their associated with the regulation of TJ protein expression, we determined the protein levels of occludin, claudin-1, and ZO-1 using immunoblotting with detergent-soluble and detergent-insoluble fractions. Figure 2A demonstrated the D-limonene treatment resulted in a significant and dose-dependent increase in the protein levels of occludin, claudin-1, and ZO-1 within the detergent-insoluble fraction of Caco-2 cells. This indicates an improvement in their binding to the actin cytoskeleton. Densitometric analysis further confirm that the levels of occludin, claudin-1, and ZO-1 in the detergent-insoluble fraction were higher in Caco-2 cell monolayers treated with 100 μM D-limonene compared to the control cells (Figure 2B). Similarly, the administration of L-limonene

led to a significant and dose-dependent elevation in the protein levels of occludin, claudin-1, and ZO-1 within the detergent-insoluble fraction (Figure 2C). A notable increase in occludin and ZO-1 proteins was observed at a treatment concentration of 100 μM (Figure 2D). However, the increase of Claudin-1 expression induced by L-limonene was comparatively lower than that of D-limonene. Interestingly, there were no detectable changes in the protein levels of occludin, claudin-1, and ZO-1 in the detergent-soluble fraction (whole cell lysate) following treatment with either D-limonene or L-limonene.

3.6 | Effect of D-limonene on TJ proteins at the transcriptional level

The mRNA levels of *occludin*, *claudin-1*, *claudin-3*, *ZO-1*, *ZO-2*, and *JAM-1* showed a time-independent increase following treatment with D-limonene for 6 h. Indeed, each gene exhibited differential expression over the course of 6–48 h. Figure 2E illustrates that *occludin* displayed a significant increase after 12 h and reached its peak at 24 h. *Claudin-1* demonstrated an initial increase after 6 h, which further intensified at 12 h and remained sustained until 24 h (Figure 2F). On the other hand, *claudin-3* showed a significant increase after 6 h, followed by a decrease at 12 h, and maintained its elevated expression until 48 h (Figure 2G). In contrast, *ZO-1* exhibited a remarkable increase in expression at 24 h, while no significant increase was observed at other time points (Figure 2H). Conversely, *ZO-2* displayed a marked increase after 6 h, which persisted until 24 h (Figure 2I). Regarding *JAM-1*, a significant increase was observed immediately after 6 h, no significant difference was noted at 12 h, and then the expression significantly increased again at 24 h (Figure 2J).

3.7 | Effect of limonene on TJs expression in inflamed intestinal epithelial cells

To further explore the effect of limonene on TJs protein expression in intestinal epithelial cells, membrane bound occludin expression was determined. Laser-scanning confocal microscopy demonstrated a notable decrease in occludin levels at the intercellular junction in cell treated with CytoMix. Conversely, treatment with 100 μM of either D-limonene or L-limonene for 48 h resulted an increased immunofluorescence intensities for occludin at the intercellular junctions, equivalent to those observed in control cell monolayers (Figure 3A). Moreover, the Caco-2 cells exposed to CytoMix exhibited a notable decrease in the mRNA expression of *occludin* and

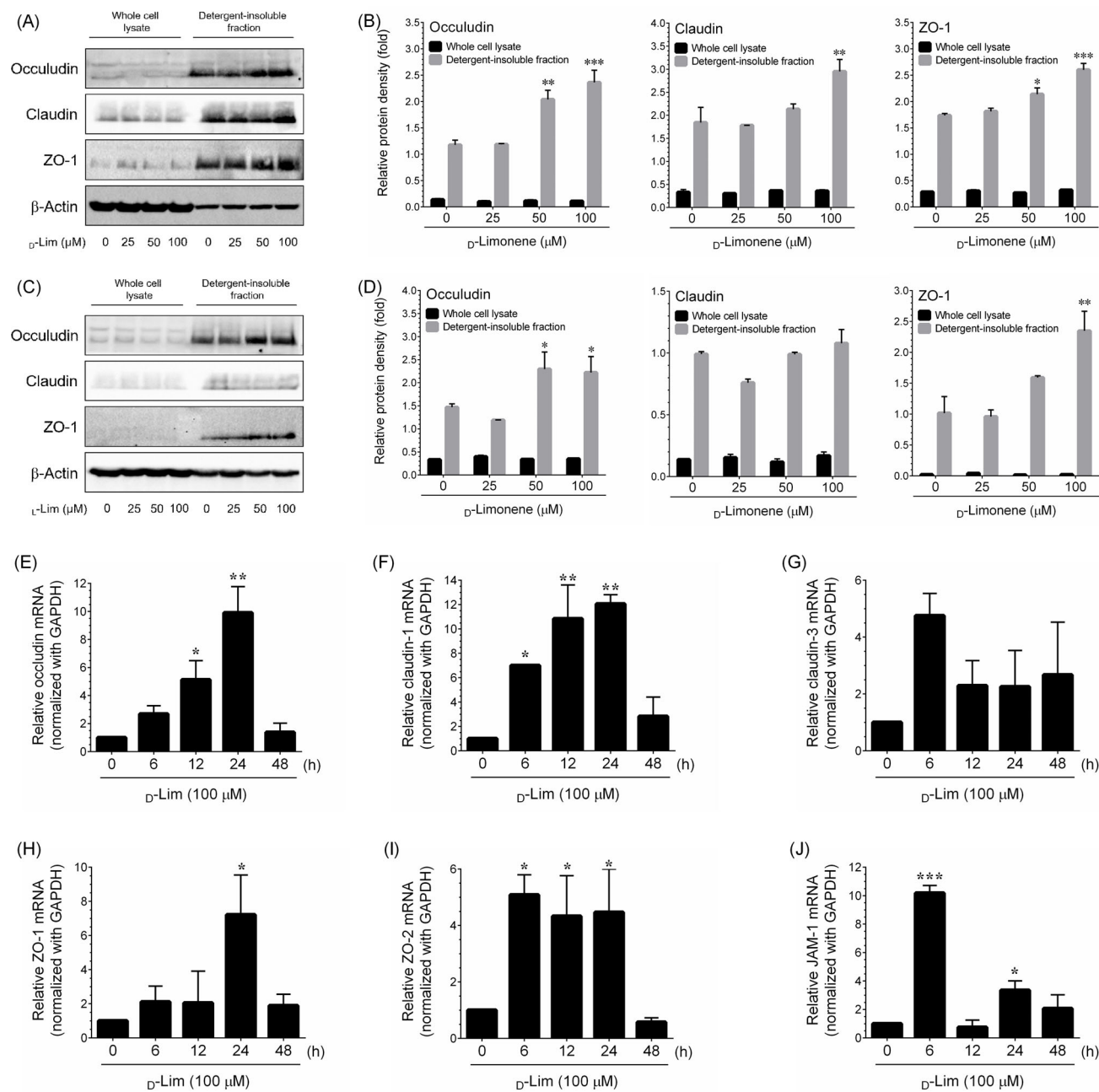


FIGURE 2 Effect of D/L -limonene on TJ protein and mRNA expression in Caco-2 cells. (A, C) Cells were incubated with various doses of D/L -limonene for 48 h. Detergent-insoluble and -soluble fractions (whole cell lysate) were prepared and immunoblotted for occludin, claudin-1, ZO-1, and β -Actin. (B, D) The histogram shows the relative protein expression levels of occludin, claudin-1, and ZO-1, which are normalized with an internal control β -Actin. (E) Immunolocalization of occludin after treatment with D/L -limonene for 48 h. After treatment, cells were fixed, and stained for occludin using specific primary and FITC-conjugated secondary antibodies. Images were obtained using a laser-scanning confocal microscope. (F–K) To quantify the mRNA expression levels of occludin, claudin-1, claudin-3, ZO-1, ZO-2, and JAM-1, Caco-2 cells were preincubated with limonene (100 μ M) for 6–48 h. Total RNA was extracted and subjected to q-PCR analysis. Relative targeted mRNA level was normalized with GAPDH mRNA. Values represent the mean \pm SD of three independent experiments. Statistical significance was denoted as * p < 0.05, ** p < 0.01, and *** p < 0.001 when comparing the D/L -limonene treatment groups to the control group.

claudin-1. However, co-treatment with D -limonene and L -limonene demonstrated significant protection against the CytoMix-induced reduction in *occludin* and *claudin-1* genes (Figure 3B,C). Certainly, in comparison to L -

limonene, D -limonene exhibited significantly more robust protective effects. These data provide positive feedback that both D -limonene and L -limonene have the capacity of improving intestinal barrier function.

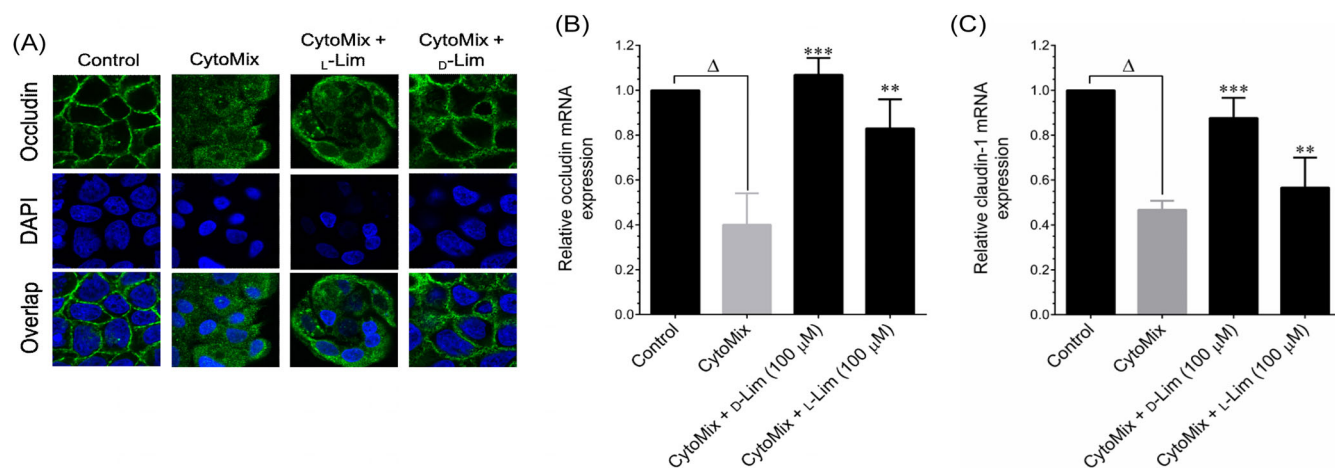


FIGURE 3 Effect of D/L-limonene on TJ protein and mRNA expression in inflamed Caco-2 cells. (A) Immunolocalization of occludin after treatment with D/L-limonene in the presence of CytoMix for 48 h was analyzed using fluorescence microscope. After treatment, cells were fixed, and stained for occludin using specific primary and FITC-conjugated secondary antibody. Images were obtained using a laser-scanning confocal microscope. (B,C) To quantify the mRNA expression levels of occludin and claudin-1, Caco-2 cells were co-incubated with D/L-limonene (100 μM) and CytoMix for 24 h. Total RNA was extracted and subjected to q-PCR analysis. Relative targeted mRNA level was normalized with GAPDH mRNA. Values represent the mean \pm SD of three independent experiments. Statistical significance was denoted as $\Delta p < 0.001$ compared to control versus CytoMix, $**p < 0.01$ and $***p < 0.001$ when comparing the D/L-limonene treatment groups to the CytoMix group.

3.8 | Effect of D-limonene on adherens junction proteins in intestinal epithelial cells

As such, D-limonene exhibited a decrease in paracellular permeability by regulating that TJ proteins. Consequently, we aim to investigate whether limonene also affects AJ proteins in Caco-2 cells. Figure 4A illustrates the results, showing that treatment with D-limonene for 48 h led to a significant and dose-dependent increase in the E-cadherin protein level. Notably, a substantial induction in the E-cadherin level was observed at 25 μM, and a maximal response was achieved at a dose of 100 μM. Moreover, 50 μM D-limonene exhibited a similar induction with 25 μM (Figure 4B). Additionally, treatment with D-limonene resulted a significant and dose-dependently down-regulated the expression of vimentin (Figure 4C). Particularly, at a dose of 100 μM D-limonene almost completely inhibited vimentin protein expression in Caco-2 cells. Furthermore, we evaluated the mRNA expression levels of *E-cadherin* and *vimentin* after 12 h incubation with D-limonene. The Q-PCR analysis revealed that D-limonene significantly increased *E-cadherin* mRNA levels. The increase was significant and dose-dependent, observed over a dose of 50 μM (Figure 4D). Similarly, D-limonene treatment down-regulated mRNA levels of *vimentin* in a dose-dependently manner (Figure 4E). These effects were consistent with the observed changes in protein levels. In summary,

these findings indicate that D-limonene enhances E-cadherin and reduces vimentin expression in intestinal epithelial cells. These effects achieved both translation and transcription processes.

3.9 | Effect of D-limonene on CB1R functions in intestinal epithelial cells

It has been well demonstrated that blocking cannabinoid receptor type-1 (CB1R) critically regulates intestinal barrier function in both animal and cell models.²⁰ To further elucidate the molecular mechanism in which D-limonene exerts its efficacy on the regulation of TJ and AJ proteins, we investigated the expression and localization of CB1R in Caco-2 cells. Initially, we evaluated the effect of limonene along with other pure compounds, including linalool, benzyl acetate, and citronellol. Among these compounds, treatment with both D- and L-limonene (100 μM) significantly inhibited CB1R expression in Caco-2 cells (Figure S4A). The inhibition occurred in a dose-dependent manner (Figure S4B,C). Notably, compared to L-limonene, D-limonene exhibited stronger CB1R expression. Therefore, we further examined the effect of D-limonene on CB1R expression. As shown in Figure 5A, treatment with D-limonene significantly and dose-dependently decreased the basal level of CB1R expression in whole cell lysate (detergent soluble fraction), while CB1R expression was hardly detectable in

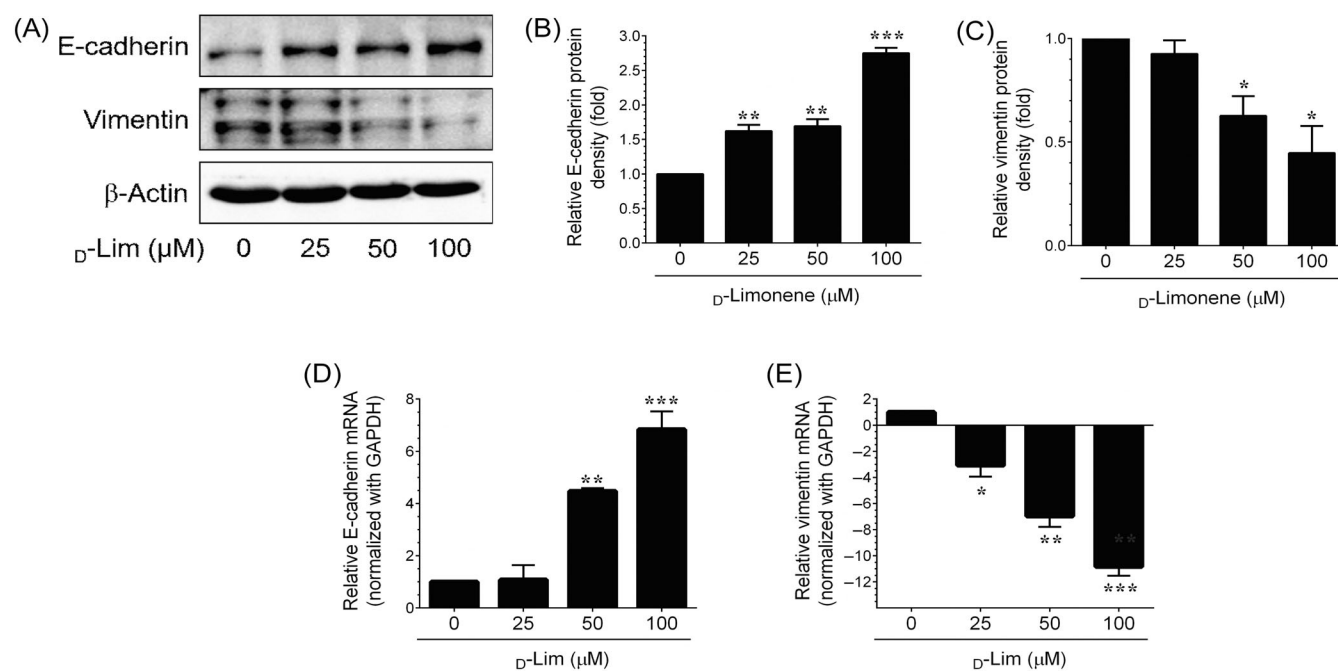


FIGURE 4 Effect of D-limonene on AJ protein and mRNA expression in Caco-2 cells. (A) Cells were incubated with various doses of D-limonene for 48 h. Whole cell lysates were prepared and immunoblotted for E-cadherin, vimentin, and β -actin. (B, C) The histogram shows the relative protein expression levels of E-cadherin, and vimentin, which are normalized with an internal control β -actin. (D, E) To quantify the mRNA expression levels of E-cadherin, and vimentin, Caco-2 cells were preincubated with various doses of D-limonene for 24 h. Total RNA was extracted and subjected to q-PCR analysis. Relative E-cadherin and vimentin mRNA levels were normalized with GAPDH mRNA. Values represent the mean \pm SD of three independent experiments. Statistical significance was denoted as * p < 0.05, ** p < 0.01, and *** p < 0.001 when comparing the D-limonene treatment groups to the control group.

detergent-insoluble fraction, showing no effect of limonene on this fraction. The histogram indicates the fold change of CB1R protein expression by D-limonene in both whole cell lysate and detergent-insoluble fractions. Based on these data, we hypothesize that D-limonene may function as allosteric or competitive inhibitor of CB1R. To further validate our hypothesis, we determined the effect of D-limonene in combination with CB1R antagonists, rimonabant and ORG27569 under CytoMix and 2-AG-stimulated conditions in Caco-2 cells. Our result demonstrated that Caco-2 cells exhibited a noteworthy decrease in TEER when stimulated with CytoMix and 2-AG (Figure 5B,C). However, the co-treatment involving D-limonene, rimonabant, and ORG27569 significantly improved TEER in both of these stimulated conditions. Nevertheless, the increase in TEER caused by ORG27569 in 2-AG-stimulated cells was not statistically significant (Figure 5C). Furthermore, a significant increase in CB1R expression was found in Caco-2 cells when exposed to 2-AG. However, co-treatment with D-limonene, rimonabant, and ORG27569 significantly reduced CB1R expression (Figure 5D). On the other hand, treatment with 2-AG remarkably increased CB1R

expression. However, when co-treatment with D-limonene, CB1R expression was significantly decreased, whereas neither ORG27569 nor rimonabant could down-regulate CB1R expression (Figure 5E). Additionally, D-limonene treatment had no significant effect on CB1R expression at the translational level (Figure S4D).

To further demonstrate the involvement of CB1R in intestinal barrier function, we established a *CB1R* gene knockdown model in Caco-2 cells through siRNA transfection. Figure 5F,G, cells transfected with scrambled siRNA (control siRNA) exhibited a significant decrease in occludin and E-cadherin mRNA levels when treated with CytoMix. However, co-treatment with D-limonene markedly prevented the CytoMix-induced reduction in occludin and E-cadherin. Conversely, in siCB1R-transfected cells, a partial reduction in occludin and E-cadherin levels was observed. Notably, D-limonene treatment in these cells led to a profound increase in occludin and E-cadherin mRNA levels. Moreover, a comparison of the effect of D-limonene on occludin and E-cadherin mRNA levels between scrambled siRNA and siCB1R-transfected cells revealed elevated levels of occludin and E-cadherin in the siCB1R transfected cells. To more comprehensively

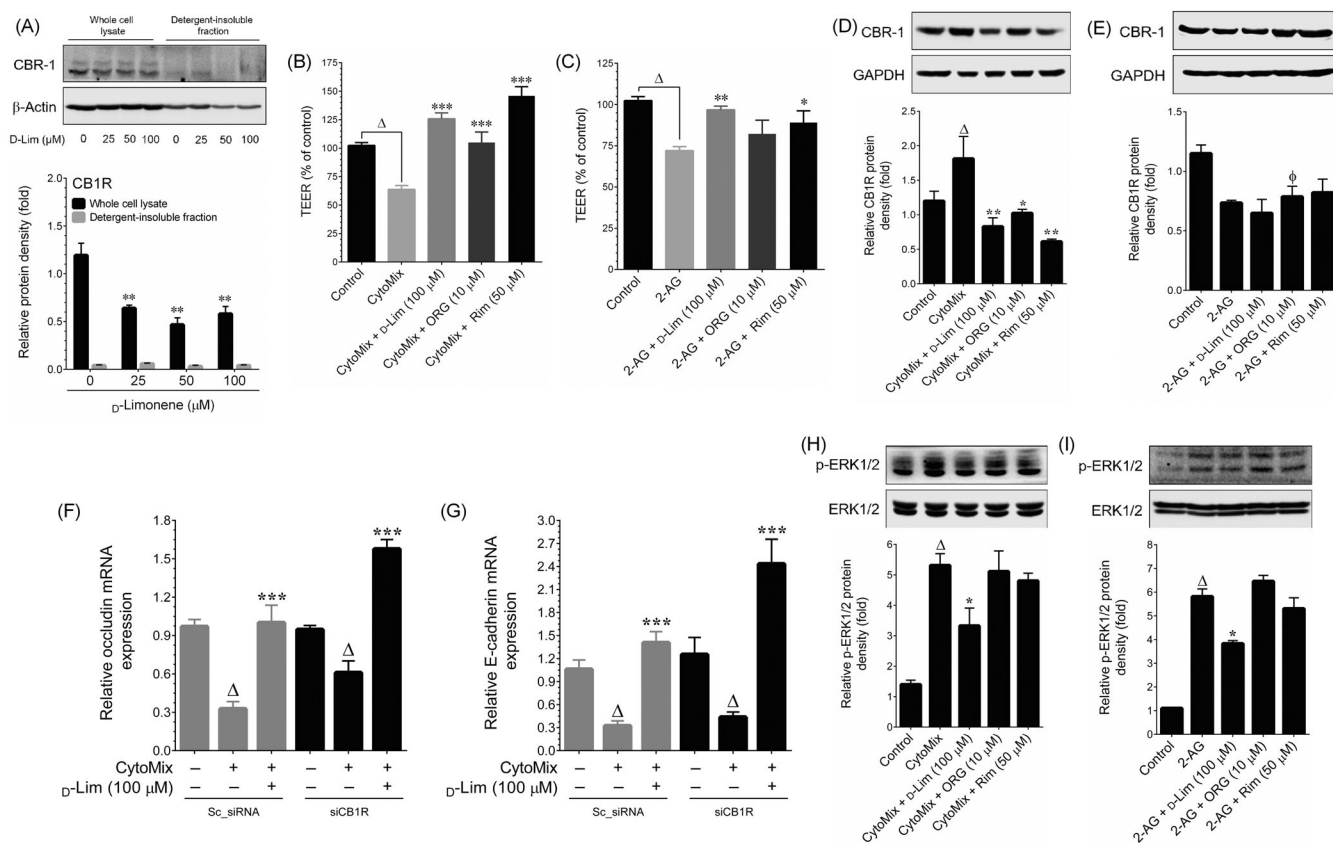


FIGURE 5 Effect of D-limonene on CB1R expression in Caco-2 cells. (A) Cells were incubated with various doses of D-limonene for 48 h. Detergent-insoluble and -soluble fractions (whole cell lysate) were prepared and immunoblotted for CB1R, and β -actin. The histogram shows the relative protein expression levels of CB1R, which is normalized with an internal control β -actin. (B, C) The Caco-2 cell monolayer barrier was disturbed by incubation with either CytoMix or 2-AG and then treated with D-limonene (D-Lim), rimonabant (Rim), or ORG27569 (ORG) for 24 h. TEER was measured at 24 h after the administration of CytoMix or 2-AG in the presence or absence of D-limonene or rimonabant, or ORG27569. (D, E) Caco-2 cells were incubated with either CytoMix or 2-AG and then treated with D-limonene (D-Lim), rimonabant (Rim), or ORG27569 (ORG) for 48 h. Whole cell lysates were prepared and immunoblotted for CB1R, and β -actin. The histogram shows the relative protein expression levels of CB1R, which is normalized with an internal control β -actin. (F, G) Caco-2 cells were transfected with a specific siRNA against CB1R or a non-silencing control (scrambled siRNA). After 24 h of transfection, the cells were incubated with or without D-limonene and were induced by CytoMix for 24 h. mRNA expression levels of occludin and E-cadherin were monitored by Q-PCR analysis. (H, I) Caco-2 cells were incubated with either CytoMix or 2-AG and then treated with D-limonene (D-Lim), rimonabant (Rim), or ORG27569 (ORG) for 1 h. ERK1/2 and its phosphorylated forms were determined by immunoblotting. The histogram shows the relative protein expression levels of phosphorylated ERK1/2, which is normalized with its total form (ERK1/2). Δ p < 0.01 compared to control versus CytoMix or 2-AG and *p < 0.05, **p < 0.01, ***p < 0.001 compared with CytoMix/2-AG alone treatment groups versus CytoMix/2-AG + sample treatment groups. ϕ p < 0.01 compared to control versus CytoMix/2-AG + sample treatment groups.

characterize the effect of D-limonene on CB1R activity, we assessed the ERK1/2 activity, a downstream target of CB1R, through western blotting. As shown in Figure 5H,I, CytoMix and 2-AG treatment markedly increased ERK1/2 phosphorylation, this activity was significantly attenuated by D-limonene. Notably, ORG24569 treatment did not alter ERK1/2 activity, while rimonabant exhibited a modest inhibitory effect, although this inhibition did not reach statistical significance. Based on these observations, we hypothesize that D-limonene may interact with CB1R in a manner similar to rimonabant or ORG24569 treatment.

3.10 | Effect of D-limonene on metabolomic alterations in Caco-2 cells

A 600 MHz 1 H-NMR analysis was utilized to examine changes in the metabolite profile between the control group and Caco-2 cells treated with D-limonene for 48 h. The tentative identification of 66 metabolites found in the Caco-2 cells was compiled and presented in Table S2. The metabolites were sourced from the human metabolome database (<https://hmdb.ca>), the biological magnetic resonance data bank (BMRB) (<https://bmrbo.io>), and relevant published literature to compare their chemical

shifts. The results indicate that cellular metabolites from the control and D-limonene treatment groups yield distinct information for the metabolite profiles in intestinal epithelial cells (Caco-2 cells), suggesting that D-limonene may potentially alter cell metabolism. Although, the ¹H-NMR spectra displayed relatively similar spectral features, differences in metabolite intensities were observed, as showed in Figure S2 (NMR spectra). However, extracting information about the metabolic shift in the studied cells solely from the acquired NMR data proved to be challenging. To gain further insights into the distinct and shared metabolite profiles between the control and D-limonene-treated cells, we performed MVDA analysis using web-based tool MetaboAnalyst 5.0 (<https://www.metaboanalyst.ca>). Based on the analysis, we identified seven metabolites that were present or absent in the control and D-limonene treated groups. Specifically, metabolites including phenylalanine, myoinositol, proline, sarcosine, histidine, and 1,1-dimethyl biguanide were found only in the D-limonene treatment group, while phosphonoacetate was found only in control group (Table S2).

MetaboAnalyst 5.0 was employed for MVDA to investigate differences in metabolite expression between the control and D-limonene treated groups. The data were initially visualized in the PLS-DA score plots to identify overall metabolic patterns between the two sample sets. The PLS-DA machine learning analysis effectively distinguished D-limonene (D-Lim) and the non-treated group (Control) based on components 1 (25.0%) and 2 (20.3%), as shown Figure 6A. The PLS-DA analysis of the entire cellular metabolites revealed the presence of two distinct clusters, with excellent reproducibility of the biological replicates evident through their close proximity in the PLS-DA score plot. The two clusters, one representing the control group (blue) and the other representing the D-limonene-treated group (yellow), were clearly separated. Furthermore, a 3D diagram of the PLS-DA score plot was presented in Figure S5.

In Figure 6B, it is evident that the variable importance in the projection (VIP) score exceeds 1, indicating its significance. To further validate this finding, we performed heatmap analysis using Ward's method. Figure 6C displays the relative concentrations of the identified metabolites, comparing them between the two samples. Different shades of color represent metabolite variations, with red indicating the highest amounts and blue representing the lowest amounts in the two sample groups. The VIP score obtained from PLS-DA corresponds to the heatmap results, reinforcing the observation that the control group exhibits notably higher levels of cellular metabolites compared to the D-limonene treatment group. The heatmap's ranking of the VIP score

metabolites aligns with the results from the PLS-DA score plot.

Additionally, a fold change (FC) analysis was conducted to compare the absolute values of change between the means of the two groups. Significant features are considered to be those with fold changes exceeding the specified threshold (2.0). As shown in Figure 6D, compared with control, D-limonene positively regulated 11 metabolites, while 9 metabolites were negatively regulated. Furthermore, the MetaboAnalyst 5.0 analysis revealed that only two metabolites showed significant differences between the control and D-limonene treatment groups, with a *p*-value <0.05. These metabolites included β-glucose and 2-oxosuccinamate (Figure 7A,B).

Indeed, the level of metabolites like β-glucose was significantly decreased in D-limonene treated cells, indicating that D-limonene promotes glucose uptake in intestinal epithelial cells. Previous studies have reported that CB1R antagonist rimonabant promotes glucose uptake in various cell types, including skeletal muscle and intestinal epithelial cells.^{21,22} Therefore, it is plausible to conclude that D-limonene's CB1R antagonistic property may support glucose uptake and energy metabolism, ultimately reading to reduction in the amount of β-glucose in the intestinal cells.

On the other hand, 2-oxosuccinamate was also significantly reduced in D-limonene treated groups. Studies have shown that glutamate is the predominant free amino acid in the brain and plays a central role in numerous metabolic pathways. During asparagine catabolic process, glutamate is broken down via the intermediate 2-oxosuccinamate. Therefore, D-limonene may stabilize intercellular levels of glutamate by decreasing 2-oxosuccinamate. However, it is important to note that this metabolic analysis does not provide substantial evidence to support the notion that D-limonene has an effect on improving intestinal barrier function.

4 | DISCUSSION

The intestinal barrier serves as a crucial protective mechanism against pathogenic microorganisms and microbial toxins. Proper functioning relies on TJ permeability and the integrity of epithelial cells, and any disruption can lead to the progression gastrointestinal and systemic diseases.²³ There is a growing body of evidence suggesting that natural products, such as plant extracts, plant volatiles, dietary phytochemicals, probiotics, and macro/micro nutrients, play a role in safeguarding the intestinal epithelium by enhancing intestinal barrier function.^{24–26}

Limonene is widely distributed among various citrus and plant species and has been identified in over

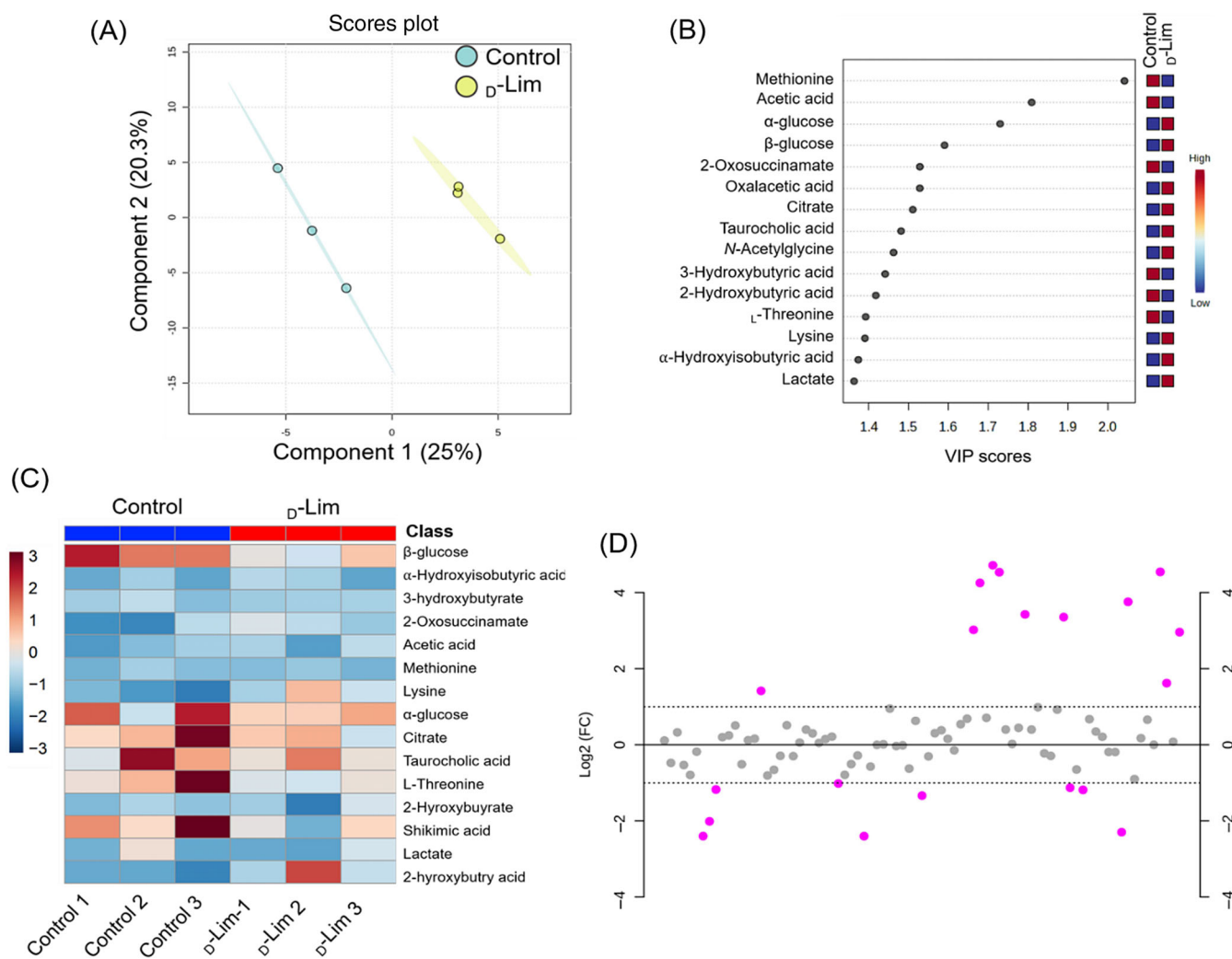


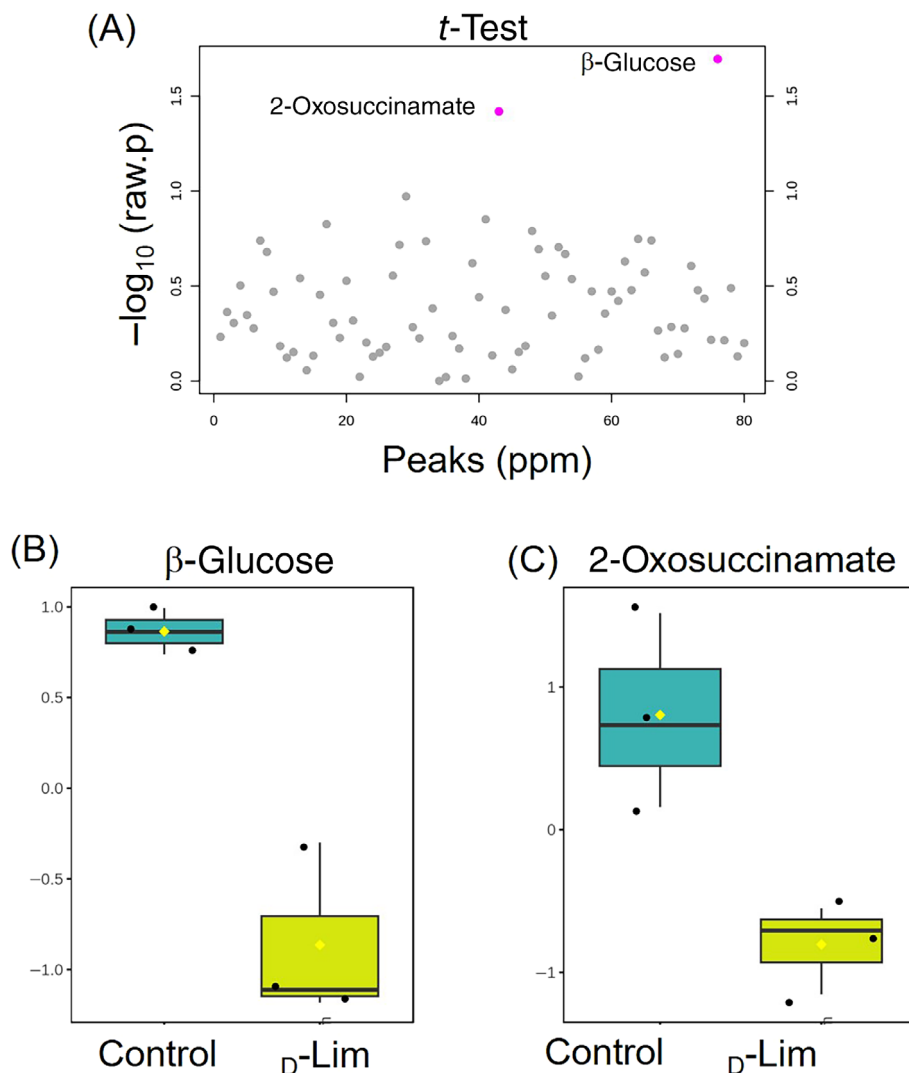
FIGURE 6 Successful separation of D-limonene treated groups from the non-treated control group. (A) In the two-dimensional PLS-DA score plots, the D-limonene treatment group (D-Lim) and non-treated group (Ctr) were effectively distinguished based on components 1 (25.6%) and 2 (18.5%). The green dots represent cells treated with 0.1% DMSO (Ctr), while the red dots represent cells treated with 100 μ M D-limonene (D-Lim). (B) Proton nuclear magnetic resonance analysis (1 H-NMR) yielded variable importance in projection (VIP) scores, and 15 significant metabolites were selected based on a VIP score >1.1 as determined by the PLS-DA model. (C) The heat map displays the expression levels of the top 15 metabolites selected by PLS-DA from the control and D-limonene-treated groups. The color-coded variation ranges from dark red (positive value of 2) to dark blue (negative value of 2), representing the highest to lowest computed ratios of metabolites. The samples are represented by green boxes for the control group (Ctr) and red boxes for the D-limonene-treated group (D-Lim). Each row corresponds to a metabolite, and each column represents a replicate. The heat map was generated using MetaboAnalyst 5.0 with Ward's method and colored boxes. The results are presented as the mean \pm standard deviation (SD) of three separate experiments.

300 essential oils, with concentrations ranging from as high as 90%–95% to lower levels. However, in the peel of citrus fruit essential oils, the main component is D-limonene, also known as (+)-limonene or R-limonene. Extensive bioactivity and pharmacological studies have been conducted with D-limonene, demonstrating various effects such as antioxidant, anti-inflammatory, anticancer, antiviral, antinociceptive, antidiabetic, gastroprotective, and antihyperalgesic properties.⁵ On the other hand, L-limonene, also identified as (–)-limonene or S-limonene, is relatively scarce in citrus fruits. It can, however,

be detected in citronella and lemongrass essential oils, albeit in small quantities ($<3\%$).² As a result, there have been limited bioactive investigations carried out with L-limonene.

According to a recent study, essential oils derived from lemon and limonene have demonstrated protective effects in mice against *E. coli*-induced intestinal injury and inflammation.¹⁴ However, the precise mechanisms underlying this regulation are not fully understood. In our recent findings, we observed that pre-treatment with limonene provides protection to skin keratinocytes

FIGURE 7 Effects of D -limonene on cellular metabolites were analyzed. Two metabolites showed significant fold changes (p -value < 0.5). The box-and-whisker plots illustrate the data with blue boxes representing control samples and red boxes representing D -limonene-treated cells (D -Lim). The metabolites, β -glucose and 2-succinamate, were notably reduced in D -limonene-treated cells compared to the control. Chemical shifts in bold were used to calculate integrals and p -values by comparing them with control groups. The results are presented as mean \pm SD of three independent experiments. * $p < 0.05$, ** $p < 0.01$, and *** $p < 0.001$ indicate significant differences between the control and D -limonene treatment groups.



against photodamage and photoaging caused by ultraviolet radiation. This protective mechanism was associated with the enhancement of barrier function through the up-regulation of TJs, including occludin and ZO-1.¹³ In this study, we presented evidence that both L - and D -limonene enhance the integrity of TJs in Caco-2 cell monolayers, which are widely used as a representation of the intestinal epithelium in various studies. The enhancement was observed through increased expression and stabilization of TJ and AJ molecules. Interestingly, the increase in TEER caused by L/D -limonene were similar to that brought about by quercetin, a plant flavonoid known to improve TJ integrity as described previously.²⁷ However, there were differences in the changes in TEER values between these two isomers of limonene.

The inflammatory response is the main cause of injury to the intestinal barrier function. Several factors have been identified to contribute to gut barrier impairment and increased permeability, with bacteria and their by-products being significant contributors.²⁸ Previous

studies have shown that bacterial byproduct LPS and interleukin- 1β (IL- 1β) can increase intestinal epithelial permeability in Caco-2 cells.^{29,30} In this investigation, we developed a pro-inflammatory cocktail called CytoMix, comprising interleukin- 1β (IL- 1β), tumor necrosis factor- α (TNF α), interferon- γ (IFN γ), and LPS. We used CytoMix to induce an in vitro intestinal epithelial barrier, as described previously.³¹ While CytoMix treatment reduced TEER in Caco-2 cells, the decrease was not statistically significant. However, it significantly increased paracellular permeability, as evident from yellow Lucifer (LY) flux. Notably, treatment with L/D -limonene exhibited a significant and dose-dependently increase TEER and a decrease LY flux in CytoMix-induced Caco-2 cells, indicating that limonene enhances intestinal barrier function in an endotoxin-independent manner.

The TJ complex is structured through specific interactions involving a diverse array of transmembrane and cytosolic proteins. The permeability of the barrier appears to be intricately regulated by the expression, distribution,

and interactions of each individual TJ protein.³² Our results demonstrated that D-limonene and L-limonene have a beneficial effect on intestinal epithelial cells, reducing barrier impairment and maintain the integrity of intestinal barrier function in inflamed cells. Furthermore, occludin, claudin, and ZO-1 represent the principal proteins of utmost importance in constituting TJs within intestinal epithelial cells and the overall integrity of the intestinal barrier.³³ Specifically, the TJs, composed of claudins, occludin, zonula occludens, connective adhesion molecules, and scaffold proteins, primarily govern paracellular transport regulation and serve as the principal structural component in establishing the barrier function of epithelial cells.³³ In a study by Ref. [14], it was reported that pretreatment with lemon essential oil and D-limonene essential oil significantly increased the expression of claudin, occludin and ZO-1 in the *E. coli*-induced mice duodenum. This study also highlights that D-limonene is a major component of both lemon (47.48%) and limonene (83.52%) essential oils. Thus, the protective effect might be attributed to D-limonene, serving as the potential bioactive component.

In our study, we found that D/L-limonene-mediated increment led to an increase in the TEER, which is indicative of improved barrier function. This effect was associated with the upregulation of key TJ regulatory proteins, including ZO-1, occludin, and claudin-1. After 48 h of D/L-limonene treatment, there was a dose-dependent increase in these proteins in the detergent-insoluble fractions, while their presence in the whole cell lysate was minimal. These findings strongly support our previous observations, where D-limonene demonstrated a significant increase in ZO-1 and occludin expression in skin keratinocytes.¹³ Interestingly, in keratinocytes, D-limonene did not show any modulation of claudin expression, whereas it notably enhanced claudin expression in intestinal epithelial cells. Confocal microscopy analysis further confirmed that D/L-limonene induced the accumulation of occludin at the intercellular junctions after 48 h of treatment. Additionally, D-limonene increased the mRNA expression of occludin, claudin-1, claudin-3, ZO-1, ZO-3, and JAM expression in Caco-2 cells. However, it is worth noting that the increase in claudin-3 mRNA expression did not reach statistical significance. Furthermore, our results suggest that the promotive effect of L-limonene on intestinal barrier function was less potent compared to D-limonene, as evidenced by TEER measurements and western blotting analyses.

Adherens junctions are protein complexes located at cell–cell contact points the lateral membrane, forming. The principal AJs are primarily composed of cadherin–catenin interactions. These cadherin–catenin complexes

play vital roles in the cell proliferation, maintaining cell polarity, regulating epithelial migration, and contributing to the formation of other adhesive complexes.³⁴ Particularly, E-cadherin plays a critical role in facilitating cell–cell adhesion and preserving the proper structure of epithelial cells. Loss of E-cadherin compromises epithelial differentiation, leading to cells acquiring a motile and invasive phenotype.³⁵ Additionally, targeted inhibition of E-cadherin using specific antibodies induces the disruption of AJs and results in increased permeability.³⁶ In our study, we observed that D-limonene treatment significantly and dose-dependently increased E-cadherin expression in Caco-2 cells. However, it is worth noting our finding contradicts to another report indicating that D-limonene decreases E-cadherin expression in colorectal cancer tissues derived from rats with dimethylhydrazine-induced colon cancer.³⁷ Vimentin, an essential member of the intermediate filament protein family (IFs), is ubiquitously expressed in normal mesenchymal cells and plays a crucial role in upholding cellular integrity and offering stress resistance.³⁸ In a previous study, vimentin expression was significantly increased in Caco-2 cells after co-incubation with pathogenic bacterium *Proteus vulgaris*. This bacterial stimulation led to an upregulation of epithelial-to-mesenchymal transition (EMT) genes, resulting in significant morphological changes in intestinal epithelial cells.³⁹ Interestingly, treatment with D-limonene significantly and dose-dependently inhibited vimentin expression in Caco-2 cells. The data presented provides compelling evidence that D-limonene has the potential to prevent cell morphological alterations and uphold cellular integrity.

The endocannabinoid system exhibits extensive expression in both rodent and human organisms, serving a myriad of physiological functions, including the regulation of gastrointestinal function. Evidence also suggests that disturbances in the endocannabinoid system may play a role in gastrointestinal disorders, such as irritable bowel syndrome, inflammatory bowel disease, and obesity.⁴⁰ In the colon, the endocannabinoid system is believed to interact with gut microbiota and regulate epithelial barrier permeability. For instance, activation of cannabinoid type 1 receptors (CB1Rs) in mice led to increased circulating levels of LPS, an endotoxin released by gram-negative bacteria. This impact is thought to occur through the reduction in the expression of TJ proteins, including occludin and zonula occludens-1, resulting in increased permeability.⁴¹ Moreover, substantial evidence supports the idea that inhibiting CB1R could improve intestinal barrier function in both animal and cell models.²⁰ Various synthetic CB1R antagonists, such as rimonabant, AM251, AM281, SR144528, AM6545, ORG27569, and Otenabant, have been developed and



function as receptor antagonists or receptor inverse antagonists.⁴²

Various plant-derived compounds that act as CBR agonists have been identified, including resorcinol derivatives, cannabidiol, cannabigerol, cannabinol, and cannabidivarin, along with their corresponding carboxylates, such as Δ^9 -tetrahydrocannabinolic acid and cannabidiolic acid.⁴² However, only a few plant-derived cannabinoids receptor antagonists have been identified. One notably example is cannabidiol, which acts as a non-competitive antagonist for CB1/CB2 receptors. Additionally, Δ^9 -tetrahydrocannabivarin (THCV) has been found to modulate the effects of tetrahydrocannabinol by directly blocking CB1 receptor and functioning as an inverse agonist.⁴³ Our study revealed that *D*-limonene treatment significantly suppresses CB1R expression at the translational level in Caco-2 cells, without affecting it at the transcriptional level. This data suggest that *D*-limonene might directly interact with CB1R leading to a reduction in its expression. To further validate this observation, we compared the CB1R inhibitory effect of *D*-limonene with that of rimonabant and ORG27569 under CytoMix and 2-AG-stimulated Caco-2 cells. Based on our data, we propose that *D*-limonene may interact with CB1R in a manner similar to rimonabant or ORG24569 treatment. Nevertheless, we acknowledge that this is a preliminary finding, and we intend to conduct more extensive investigations in the future to elucidate the interaction between *D*-limonene and CB1R.

Metabolic fingerprints are novel techniques used to assess the biochemical condition of a living organism by employing ¹H-NMR and MVDA. This method enables rapidly evaluation changes in health or disease conditions, as reflected in the modifications of metabolic patterns.⁴⁴ Increasingly, studies have reported that dietary phytochemicals can alter or regulate cellular metabolites in intestinal epithelial cells. Typically, metabolic fingerprinting relies on *in vivo* studies, which can be labor-intensive and costly. In contrast, *in vitro* studies offer an appealing alternative as they are not hindered by these drawbacks.⁴⁴

In our study, we incubated matured Caco-2 cells with *D*-limonene for 48 h, and then analyzed the resulting cell fractions using ¹H-NMR followed by MVDA.

D-Limonene treated cells showed clear differences compared to cells exposed to 0.1% DMSO (control) after 48 h. Our studied results indicated that the impact of *D*-limonene on Caco-2 cells was mainly attributed to the interplay between glucose metabolism and glutamate. This was evidenced by the observed reduction in β -glucose and 2-succinamate levels in *D*-limonene-treated cells. It is reasonable to conclude that *D*-limonene might stimulate glucose uptake and energy metabolism, given

the known effect of the CB1R antagonist, rimonabant, which enhances glucose uptake in various cell types, including skeletal muscle and intestinal epithelial cells.^{21,22} Conversely, in the *D*-limonene treated groups, there was a significant reduction in 2-oxosuccinamate. Glutamate is the brain's most abundant free amino acid and plays a crucial role at the intersection of various metabolic pathways. In the process of asparagine catabolism, glutamate is broken down through the intermediate 2-oxosuccinamate. Consequently, *D*-limonene appears to stabilize intracellular glutamate levels by decreasing 2-oxosuccinamate. Despite the metabolic analysis, there is insufficient evidence to substantiate the idea that *D*-limonene has a positive impact on enhancing intestinal barrier function.

In conclusion, our study demonstrated that both *D*-limonene and *L*-limonene had a significantly and dose-dependently increased transepithelial electrical resistance (TEER) in Caco-2 cell monolayers. *D*-Limonene exhibited a stronger effect in enhancing TJ integrity compared to *L*-limonene. Additionally, both *D*-limonene and *L*-limonene promoted the healing and recovery of inflamed epithelial cell monolayers, as evidenced by the increase in TEER values after 48 h of treatment. Furthermore, *D*-limonene demonstrated greater efficacy in regulating TJ and AJ proteins in intestinal epithelial cells by inhibiting cannabinoid receptor type-1 (CB1R) expression, compared to *L*-limonene, *D*-limonene. Under inflammatory and 2-AG-stimulated conditions, *D*-limonene exhibited stronger effects in decreasing CB1R expression and improving TEER, suggesting a potential allosteric or competitive inhibition of CB1R by *D*-limonene. Moreover, ¹H-NMR analysis and MVDA revealed distinct metabolite profiles between the control and *D*-limonene-treated groups in Caco-2 cells. *D*-Limonene showed an inhibitory effect on CB1R expression and a potential influence on glucose uptake and glutamate metabolism in intestinal epithelial cells. These findings suggest that *D*-limonene could be a promising agent for enhancing intestinal epithelial barrier function. However, further research, including *in vivo* studies, is required to fully elucidate its mechanism of action.

AUTHOR CONTRIBUTIONS

Conceptualization, S.Y.W. Methodology, K.J.S.K. Investigation, K.J.S.K, M.G.V and G.D. Validation, K.J.S.K. Formal analysis, K.J.S.K. and G.D. Writing original draft, K.J.S.K. Writing review & editing, K.J.S.K and S.Y.W. Supervision, S.Y.W. Funding, S.Y.W.

ACKNOWLEDGMENTS

This study was supported by grants from the National Science and Technology Council (NSTC), Taiwan

(109-2313-B-005-043-MY3). The funding body did not have any role in the design of the study and collection, analysis, and interpretation of data and in writing the manuscript.

CONFLICT OF INTEREST STATEMENT

All authors declare no conflicts of interest.


DATA AVAILABILITY STATEMENT

The data that support the findings of this study are available from the corresponding author upon reasonable request.

ORCID

K. J. Senthil Kumar  <https://orcid.org/0000-0002-8310-0546>

M. Gokila Vani  <https://orcid.org/0000-0001-6111-6187>

Sheng-Yang Wang  <https://orcid.org/0000-0002-8579-3569>

REFERENCES

- AlSaffar RM, Rashid S, Ahmad SB, Rehman MU, Hussain I, Parvaiz Ahmad S, et al. D-limonene (5 (one-methyl-four-[1-methylethenyl]) cyclohexane) diminishes CCl₄-induced cardiac toxicity by alleviating oxidative stress, inflammatory and cardiac markers. *Redox Rep.* 2022;27(1):92–9.
- Kvittingen L, Sjursnes BJ, Schmid R. Limonene in citrus: a string of unchecked literature citations? *J Chem Ed.* 2021;98(11):3600–7.
- Ibáñez MD, Sanchez-Ballester NM, Blázquez MA. Encapsulated limonene: a pleasant lemon-like aroma with promising application in the agri-food industry. A review. *Molecules.* 2020;25(11):2598.
- Vieira AJ, Beserra FP, Souza MC, Totti BM, Rozza AL. Limonene: aroma of innovation in health and disease. *Chem Biol Int.* 2018;283:97–106.
- Anandakumar P, Kamaraj S, Vanitha MK. D-limonene: a multifunctional compound with potent therapeutic effects. *J Food Biochem.* 2021;45(1):e13566.
- Kim YW, Kim MJ, Chung BY, Bang du Y, Lim SK, Choi SM, et al. Safety evaluation and risk assessment of d-limonene. *J Toxicol Environ Health B Crit Rev.* 2013;16(1):17–38.
- Stolfi C, Maresca C, Monteleone G, Laudisi F. Implication of intestinal barrier dysfunction in gut dysbiosis and diseases. *Bio-medicine.* 2022;10(2):289.
- Chelakkot C, Ghim J, Ryu SH. Mechanisms regulating intestinal barrier integrity and its pathological implications. *Exp Mol Med.* 2018;50(8):1–9.
- Izzo AA. The cannabinoid CB₂ receptor: a good friend in the gut. *Neurogastroenterol Motil.* 2007;19(9):704–8.
- Wright KL, Duncan M, Sharkey KA. Cannabinoid CB₂ receptors in the gastrointestinal tract: a regulatory system in states of inflammation. *Br J Pharmacol.* 2008;153(2):263–70.
- Gigli S, Seguela L, Pesce M, Bruzzese E, D'Alessandro A, Cuomo R, et al. Cannabidiol restores intestinal barrier dysfunction and inhibits the apoptotic process induced by Clostridium difficile toxin a in Caco-2 cells. *United European Gastroenterol J.* 2017;5(8):1108–15.
- Sambuy Y, De Angelis I, Ranaldi G, Scarino ML, Stammati A, Zucco F. The Caco-2 cell line as a model of the intestinal barrier: influence of cell and culture-related factors on Caco-2 cell functional characteristics. *Cell Biol Toxicol.* 2005;21(1):1–26.
- Kumar KJS, Vani MG, Wang SY. Limonene protects human skin keratinocytes against UVB-induced photodamage and photoaging by activating the Nrf2-dependent antioxidant defense system. *Environ Toxicol.* 2022;37(12):2897–909.
- Zhao C, Zhang Z, Nie D, Li Y. Protective effect of lemon essential oil and its major active component, D-limonene, on intestinal injury and inflammation of E. coli-challenged mice. *Front Nutr.* 2022;9:9.
- Jendoubi T. Approaches to integrating metabolomics and multi-omics data: a primer. *Metabolites.* 2021;11(3):184.
- Zhang A, Sun H, Xu H, Qiu S, Wang X. Cell metabolomics. *Omic.* 2013;17(10):495–501.
- Qiu S, Cai Y, Yao H, Lin C, Xie Y, Tang S, et al. Small molecule metabolites: discovery of biomarkers and therapeutic targets. *Signal Transduct Target Ther.* 2023;8(1):132.
- Dietmair S, Timmins NE, Gray PP, Nielsen LK, Krömer JO. Towards quantitative metabolomics of mammalian cells: development of a metabolite extraction protocol. *Anal Biochem.* 2010;404(2):155–64.
- Luo X, Gu X, Li L. Development of a simple and efficient method of harvesting and lysing adherent mammalian cells for chemical isotope labeling LC-MS-based cellular metabolomics. *Anal Chim Acta.* 2018;1037:97–106.
- Muccioli GG, Naslain D, Bäckhed F, Reigstad CS, Lambert DM, Delzenne NM, et al. The endocannabinoid system links gut microbiota to adipogenesis. *Mol Syst Biol.* 2010;6:392.
- Esposito I, Proto MC, Gazzero P, Laezza C, Miele C, Alberobello AT, et al. The cannabinoid CB₁ receptor antagonist rimonabant stimulates 2-deoxyglucose uptake in skeletal muscle cells by regulating the expression of phosphatidylinositol-3-kinase. *Mol Pharmacol.* 2008;74(6):1678–86.
- Ussar S, Haering MF, Fujisaka S, Lutter D, Lee KY, Li N, et al. Regulation of glucose uptake and enteroendocrine function by the intestinal epithelial insulin receptor. *Diabetes.* 2017;66(4):886–96.
- Li BR, Wu J, Li HS, Jiang ZH, Zhou XM, Xu CH, et al. In vitro and in vivo approaches to determine intestinal epithelial cell permeability. *J Vis Exp.* 2018;140:57032.
- Suzuki T. Regulation of the intestinal barrier by nutrients: the role of tight junctions. *Anim Sci J.* 2020;91(1):e13357.
- Rose EC, Odle J, Blikslager AT, Ziegler AL. Probiotics, prebiotics and epithelial tight junctions: a promising approach to modulate intestinal barrier function. *Int J Mol Sci.* 2021;22(13):6729.
- Lee B, Moon KM, Kim CY. Tight junction in the intestinal epithelium: its association with diseases and regulation by phytochemicals. *J Immunol Res.* 2018;2018:2645465.
- Suzuki T, Hara H. Quercetin enhances intestinal barrier function through the assembly of zonula [corrected] occludens-2, occludin, and claudin-1 and the expression of claudin-4 in Caco-2 cells. *J Nutr.* 2009;139(5):965–74.
- Massier L, Blüher M, Kovacs P, Chakaroun RM. Impaired intestinal barrier and tissue bacteria: pathomechanisms for metabolic diseases. *Front Endocrinol.* 2021;12:616506.



29. Al-Sadi RM, Ma TY. IL-1beta causes an increase in intestinal epithelial tight junction permeability. *J Immunol.* 2007;178(7):4641–9.
30. Nighot M, Al-Sadi R, Guo S, Rawat M, Nighot P, Watterson MD, et al. Lipopolysaccharide-induced increase in intestinal epithelial tight permeability is mediated by toll-like receptor 4/myeloid differentiation primary response 88 (MyD88) activation of myosin light chain kinase expression. *Am J Pathol.* 2017;187(12):2698–710.
31. Mohebal N, Ekat K, Kreikemeyer B, Breitrück A. Barrier protection and recovery effects of gut commensal bacteria on differentiated intestinal epithelial cells in vitro. *Nutrients.* 2020;12(8):2251.
32. Heinemann U, Schuetz A. Structural features of tight-junction proteins. *Int J Mol Sci.* 2019;20(23):6020.
33. Zeisel MB, Dhawan P, Baumert TF. Tight junction proteins in gastrointestinal and liver disease. *Gut.* 2019;68(3):547–61.
34. Groschwitz KR, Hogan SP. Intestinal barrier function: molecular regulation and disease pathogenesis. *J Allergy Clin Immunol.* 2009;124(1):3–20. quiz 21–22, 20.
35. Schneider MR, Dahlhoff M, Horst D, Hirschi B, Trülsch K, Müller-Höcker J, et al. A key role for E-cadherin in intestinal homeostasis and Paneth cell maturation. *PLoS One.* 2010;5(12):e14325.
36. Greenspon J, Li R, Xiao L, Rao JN, Sun R, Strauch ED, et al. Sphingosine-1-phosphate regulates the expression of adherens junction protein E-cadherin and enhances intestinal epithelial cell barrier function. *Dig Dis Sci.* 2011;56(5):1342–53.
37. Liu Y, Li Y, Yu G, Liu Y, Yang H. Impact of D-limonene on the expressions of E-cadherin and β -catenin in colorectal cancer in rats. *Anat Res.* 2008;30(5):333–5.
38. Kuburich NA, den Hollander P, Pietz JT, Mani SA. Vimentin and cytokeratin: good alone, bad together. *Semin Cancer Biol.* 2022;86:816–26.
39. Wachsmannova L, Stevurkova V, Ciernikova S. Changes in SNAI1 and VIM gene expression in Caco2 cells after cocultivation with bacteria from colorectal cancer biopsies. *Neoplasma.* 2019;66(2):271–5.
40. Hryhorowicz S, Kaczmarek-Ryś M, Zielińska A, Scott RJ, Słomski R, Pławski A. Endocannabinoid system as a promising therapeutic target in inflammatory bowel disease—a systematic review. *Front Immunol.* 2021;12:790803.
41. DiPatrizio NV. Endocannabinoids in the gut. *Cannabis Cannabinoid Res.* 2016;1(1):67–77.
42. Hourani W, Alexander SPH. Cannabinoid ligands, receptors and enzymes: pharmacological tools and therapeutic potential. *Brain Neurosci Adv.* 2018;2:2398212818783908.
43. McPartland JM, Duncan M, Di Marzo V, Pertwee RG. Are cannabidiol and $\Delta(9)$ -tetrahydrocannabinol negative modulators of the endocannabinoid system? A systematic review. *Br J Pharmacol.* 2015;172(3):737–53.
44. Lamers R-JAN, Wessels ECHH, van de Sandt JJM, Venema K, Schaafsma G, van der Greef J, et al. A pilot study to investigate effects of inulin on Caco-2 cells through in vitro metabolic fingerprinting. *J Nutr.* 2003;133(10):3080–4.

SUPPORTING INFORMATION

Additional supporting information can be found online in the Supporting Information section at the end of this article.

How to cite this article: Senthil Kumar KJ, Gokila Vani M, Dakpa G, Wang S-Y. Dietary limonene promotes gastrointestinal barrier function via upregulating tight/adherens junction proteins through cannabinoid receptor type-1 antagonistic mechanism and alters cellular metabolism in intestinal epithelial cells. *BioFactors.* 2024. <https://doi.org/10.1002/biof.2106>